5th International Supercritical CO_2 Power Cycles Symposium

March 29 - 31, 2016, San Antonio, Texas

Thermodynamic model investigation for supercritical CO_2 Brayton cycle for coal-fired power plant application

Qiao Zhao
Ph.D. Candidate
EdF R&D Department
Qiao.zhao@edf.fr
Thibaut Neveux
Research Engineer, Ph.D.
EdF R&D Department
thibaut.neveux@edf.fr
Jean-Noël JAUBERT
Professor
LRGP-CNRS
jean-noel.jaubert@univ-lorraine.fr

Mounir Mecheri
Research Engineer
EdF R&D Department
mounir.mecheri@edf.fr
Romain Privat
University Lecturer
LRGP-CNRS
Romain.Privat@univ-lorraine.fr

Qiao Zhao is PhD student at EDF R&D department. She received her M.S. in chemical engineering in ENSIACET, Toulouse. The topic of her thesis focuses on the design and conception of a Supercritical-CO_2 Brayton cycle for coal-fired plants.

ABSTRACT

Restrictive policies on greenhouse gas emissions and the drastic increase of the energy demand lead to more researches in coal-fired power plants enhancement. Preliminary studies based on process modeling show that the use of recompression Supercritical CO_2 (S-CO_2) Brayton cycle in coal-fired power plants could increase the plant efficiency in comparison with steam coal power plants. However, a more detailed study on thermodynamic models is necessary to avoid potential uncertainties in CO_2 physical property estimation, especially near its critical point. This study focuses on the following thermodynamic model investigation for S-CO_2: calculations made with six candidate equations of state (EoS) are compared with CO_2 experimental data taken from the latest release of the DECHEMA® Detherm database. The Span-Wagner (SW) equation of state turns out to be able to accurately predict CO_2 physical properties (density, heat capacity and speed of sound) of CO_2 at both high temperature, high pressure but also in the vicinity of the critical point.

INTRODUCTION

Since the 1970's, equations of state (EoS) for both pure CO_2 and its mixtures at high temperature and high pressure have been widely investigated because of their important role in geological and petroleum science. Despite these investigations, it is difficult to find a thermodynamic model that accurately predicts the CO_2 behavior in both transcritical and supercritical region because most of the EoS are inaccurate in predicting the CO_2 properties in the vicinity of its critical point. Furthermore, some equations were only designed to accurately reproduce one kind of data, e.g. Pressure-Volume-Temperature (P-v-T) properties, and suffer of inaccuracy in the prediction of other properties, e.g., enthalpy, heat capacity, sound velocity ... Given that the precision of predicted properties directly affects the mass, energy and entropy balances, and thus efficiency calculations in power cycles, the choice of an appropriate EoS is determinant for modeling and predicting the S-CO_2 power cycle behavior. Therefore, the purpose of this study is to identify the most appropriate equation of state for pure CO_2 that predicts accurately the CO_2 physical properties at both high temperature, high pressure as well as in the vicinity of its critical point.

Each EoS has more or less advantages and limitations. Conventional equations for non-polar fluid such as cubic EoS (Soave, 1972; Peng and Robinson, 1976) could successfully approximate all kinds of real fluids behavior with reasonable uncertainties and are relatively easy to compute. However, they have limited accuracy in predicting the liquid molar volumes (the liquid phase density and other properties involving the liquid molar volume). Empirical EoS, such as the virial-type EoS (Benedict et al., 1942; Starling, 1971; Nushiumi and Saito, 1975; Pitzer and Curl, 1957), predict liquid molar volumes more accurately than cubic EoS. On the other hand, the SAFT-type equations (Gross et al., 2001; Blas and Vega, 1997; Gil-Villegas et al., 1997) better predict liquid phase density than cubic EoS, but usually exhibit severe deviation in terms of critical property prediction (T_c , P_c and v_c). Specific adjustable EoS developed for CO_2, e.g., EoS expressed in terms of Helmholtz energy (Span and Wagner, 1994; Kim, 2007; Mazzoccoli et al., 2014; Yu et al., 2015), offer satisfactory prediction of each property in any regions of temperature and pressure, including the critical region.

METHODOLOGY

In this study, the six studied EoS are: Peng-Robinson (PR); Peng-Robinson with Boston-Mathias alpha function (PR-BM); Soave modified Redlich-Kwong (SRK); Lee-Kesler-Plöcker (LKP), Benedict-Webb-Rubin modified by Starling and Nushiumi (BWRS) and Span-Wagner (SW). Their functional form and the related parameters are presented in Table 1:

Equation	Function Form	Parameters
PR	$P = \frac{RT}{v-b} - \frac{a}{v(v+b)+b(v-b)}$	$a = 0.45724\frac{R^2T_c^2}{P_c}\alpha(T)$, $b = 0.07780\frac{RT_c}{P_c}$(i) $\alpha(T) = [1 + m(1 - T_r^{0.5})]^2$(ii) $m = 0.37464 + 1.54226\omega - 0.26992\omega^2$(iii) $Tr = \frac{T}{T_c}$ and $\omega = -log_{10}(\frac{P^s}{P_c}) - 1$ where P_s is the saturation vapor pressure at $Tr = 0.7T_c$
PR-BM	$P = \frac{RT}{v-b} - \frac{a}{v(v+b)+b(v-b)}$	For $Tr = \frac{T}{T_c} \leq 1$: $\alpha(T)$ is given by Eqs (ii) and (iii) For $Tr = \frac{T}{T_c} > 1$: $\alpha(T) = [exp[c(1-T_r^d)]]^2$ $d = 1 + (\frac{m}{2})$, $c = 1 - \frac{1}{d}$
SRK	$P = \frac{RT}{v-b} - \frac{a}{v(v+b)}$	$a = 0.42747\frac{R^2T_c^2}{P_c}\alpha(T)$, $b = 0.08664\frac{RT_c}{P_c}$ $\alpha(T) = [1 + m(1 - T_r^{0.5})]^2$ $m = 0.48508 + 1.55171\omega - 0.15613\omega^2$
BWRS	$P = \rho RT + (B_0RT - A_0 - \frac{C_0}{T^2} + \frac{D_0}{T^3} - \frac{E_0}{T^4})\rho^2 +$ $(b'RT - a' - \frac{d'}{T} - \frac{e'}{T^4} - \frac{f'}{T^{23}})\rho^3 +$ $\alpha'(a' + \frac{d'}{T} + \frac{e'}{T^4} + \frac{f'}{T^{23}})\rho^6 +$ $(\frac{c'}{T^2} + \frac{g'}{T^8} + \frac{h'}{T^{17}})\rho^3(1 + \gamma'\rho^2)e^{(-\gamma'\rho^2)}$	$\rho_c B_0 = A_1 + B_1\omega$, $\frac{\rho_c A_0}{RT_c} = A_2 + B_2\omega + 0.095\omega^3$ $\frac{\rho_c C_0}{RT_c^3} = A_3 + B_3\omega$, $\rho_c^2\gamma = A_4 + B_4\omega$, $\rho_c^2 b = A_5 + B_5\omega$, $\frac{\rho_c^2 a}{RT_c} = A_6 + B_6\omega$ $\rho_c^3\alpha = A_7 + B_7\omega$, $\frac{\rho_c^2 c}{RT_c^3} = A_8 + B_8\omega$, $\frac{\rho_c D_0}{RT_c^4} = A_9 + B_9\omega$ $\frac{\rho_c^2 d}{RT_c^2} = A_{10} + B_{10}\omega$, $\frac{\rho_c E_0}{RT_c^5} = A_{11} + B_{11}\omega e^{(-3.8\omega)}$ $\frac{\rho_c^2 e}{RT_c^5} = A_{12} + B_{12}\omega + C_{12}\omega^2 + D_{12}e^{(E_{12}\omega + F_{12}\omega^2)}$ $\frac{\rho_c^2 f}{RT_c^{24}} = A_{13} + B_{13}\omega + C_{13}\omega^2 + D_{13}e^{(E_{13}\omega + F_{13}\omega^2)}$ $\frac{\rho_c^2 g}{RT_c^9} = A_{14} + B_{14}\omega + D_{14}e^{(E_{14}\omega)}$ $\frac{\rho_c^2 h}{RT_c^{18}} = A_{15} + B_{15}\omega + D_{15}e^{(E_{15}\omega)}$ The values for the parameters γ', α, $A_j$and B_j (j = 1, 2, . . ., 15), $C_j$and F_j (j = 12,13) $D_j$and E_j (j = 12,...15), $a', b'...h'$ are reported in *ProsimPlus*
LKP	$Z = Z^0 + \frac{\omega}{\omega_R}(Z^R - Z^0)$ $Z^0$and Z^R are functions of the BWR form, Z^0 is for a simple fluid (argon, krypton and methane) and $Z^R$is for reference fluid(n-octane) Z^0 *or* $Z^R = 1 + \frac{B}{v_r} + \frac{C}{v_r^2} + \frac{D}{v_r^5} +$ $\frac{c_4}{T_r^3 v_r^2} + (\beta + \frac{\gamma}{v_r^2})e^{(-\frac{\gamma}{v_r^2})}$	$v_r = \frac{P_c v}{RT_c}$, $B = b_1 - \frac{b_2}{T_r} - \frac{b_3}{T_r^2} - \frac{b_4}{T_r^3}$ $C = c_1 - \frac{c_2}{T_r} - \frac{c_3}{T_r^2}$, $D = d_1 + \frac{d_2}{T_r}$ The values of b_1, b_2, b_3, b_4, c_1, c_2, c_3, c_4 , d_1, d_2,γ, β both for simple and reference fluid, are those in *ProsimPlus*
SW	$\frac{A(\rho,T)}{(RT)} = \varphi(\delta,\tau) = \varphi^\circ(\delta,\tau) + \varphi^r(\delta,\tau)$ $\varphi^\circ(\delta,\tau) = ln(\delta) + a^\circ_1 + a^\circ_2\tau + a^\circ_3 ln(\tau)$ $+ \sum_{i=4}^{8} a^\circ_i ln[1 - e^{(-\tau\theta_i{}^\circ)}]$ $\varphi^r = \sum_{i=1}^{7} n_{i,j}\delta^{d_i}\tau^{t_i} + \sum_{i=8}^{34} n_{i,j}\delta^{d_i}\tau^{t_i}e^{-\delta^{c_i}} +$ $\sum_{i=35}^{39} n_i\delta^{d_i}\tau^{t_i}e^{-\alpha_i(\delta-\varepsilon_i)^2-\beta_i(\tau-\gamma_i)^2} +$ $\sum_{i=40}^{42} n_i\Delta^{b_i}\delta e^{-C_i(\delta-1)^2-D_i(\tau-1)^2}$	$\delta = \frac{\rho}{\rho_c}$, $\tau = \frac{T_c}{T}$ $\Delta = \{(1-\tau) + A_i[(\delta-1)^2]^{1/(2\beta)_i}\}^2 + B_i[(\delta-1)^2]^{a_i}$ the coefficients and exponents of this equation can be found in Span-Wagner,1994

Table 1: Summary of the studied EoS

In order to identify an equation of state suitable for modelling the S-CO_2 power cycle, all the thermodynamic properties likely to be involved in the simulation process model need to be compared with available experimental data. Density is an important input property for numerous

unit operations of the S-CO_2 process and is thus classically considered. Contrary to the density, the speed of sound and heat capacities are "derived EoS properties", i.e., their expressions involve temperature-derivatives or density-derivatives. Heat capacities are temperature-derivatives of the enthalpy at constant pressure or temperature while the speed of sound is a function of density-derivative of the pressure at constant entropy (see Annexes). Speeds of sound and heat capacities were thus considered for evaluating the capacity of the studied EoS to predict derived properties.
From an experimental point of view, speeds of sound and densities have higher achievable precision (at least one order of magnitude higher) than most other properties, Scalabrin et al. (2007) and are thus of particular interest for our purpose. However, accessible speed of sound data are unfortunately limited in the open literature. Due to their diverging behavior, heat capacities are known to be very hard to measure in the vicinity of the critical point explaining the lack of experimental data in this area. Transport properties such as viscosity were not considered because they cannot be directly estimated from an EoS. Eventually, **the density**, the **heat capacity** and the **speed of sound** were selected as "comparison criteria" to evaluate the accuracy of the selected EoS accuracy.

The procedure of comparison consists in three steps as follows:

- **Step 1**: First, the values of the critical temperature, critical pressure and critical density of pure CO_2 calculated by the various EoS are compared with the values found in the Design Institute for Physical Properties 801 database (DIPPR, 2016) available in the DIADEM software.
- **Step 2**: Then, the comparison criteria (density, heat capacity and speed of sound) are calculated with all the studied EoS in the vicinity of the critical point (T=300-310 K, P=7.38 MPa) and are then compared with the available experimental data in Detherm (database, 2016); the EoS leading to the smallest relative "model/experimental measurement" deviations is then selected for the step 3.
- **Step 3**: The aim is to validate the selected EoS (from step 2) in the whole region of study (T=300-900 K, P=7-20 MPa) by comparing the values of the criteria (density, heat capacity and speed of sound) returned by the EoS with experimental data in this extended area.
- **Step 4**: The aim of this step is to show the comparison of EoS calculated criteria with experimental data that have been recently measured (available in Detherm database), after the publication of the Span and Wagner (1996) EoS.

While using the Detherm database, the discrimination of data is also considered since experimental data are abundant. In the entire range of study (T=300-900 K, P=7-20 MPa) in the step 3, Detherm provides 2641 "density" points, 359 "heat capacity" points and 138 "speed of sound" points.

Among all the data included, one set data referenced as Nowak et al. (1997) on density has been wrongly entered in the Detherm (10 "density" points). After investigation, the pressures recorded in the publication appear to not meet the range of our study.

Another set of data referenced in the publication of Tsuji et al. (1998) have been wrongly converted in terms of unit by the Detherm (68 "density" points). In order to cover these points in this study, the density based on the value of compressibility measured by Tsuji et al. (1998) have been recalculated. Therefore, in terms of density, 2631 points have been considered in the comparison.

In the step 2, 51 density experimental points, 14 heat capacity experimental points and 16 speed of sound experimental points are considered. In other steps (including step 2), none of experimental point is eliminated since few experimental values show important deviation outside the vicinity of the critical point and they do not seem to have a significant influence on the mean deviation calculation as long as large quantity of data are considered.

RESULTS AND DISCUSSION

1) *Step 1: EoS calculated CO_2 critical values*

Table 2 provides the critical temperature (T_c), pressure (P_c) and density (ρ_c) values returned by the various EoS. Except for the SW EoS, all the EoS use the experimental values of T_c and P_c as input parameters and consequently, returned critical temperature and pressure rigorously equal to their experimental values provided by DIPPR.

	Critical temperature (T_c/K)	Critical Pressure (P_c/MPa)	Critical density (ρ_c/kg/m^3)	$\Delta\rho$%
SW	304.13	7.3773	467.6	0.1
PR	304.21	7.3830	416.9	10.9
SRK	304.21	7.3830	385.4	17.7
LKP	304.21	7.3830	468.5	0.1
BWRS	304.21	7.3830	423.9	9.5
$\Delta\%$ *is defined as the mean average of* $100\% \cdot (\rho_{DIPPR} - \rho_{EoS\,calculated})/\rho_{DIPPR}$				
DIPPR	304.21	7.3830	468.2	-

Table 2: Critical conditions comparison from different equations of state

Table 2 shows that the SW and LKP EoS exhibit the smallest overall deviations on critical density (0.1 %) compared with the value in DIPPR database. The PR / PR-BM and BWRS EoS predict similar underestimated values of critical densities. The SRK EoS shows the biggest overall deviation (18 %) which reflects its inadequacy to reproduce the critical density.

2) *Step 2: model/experimental data comparison near the CO_2 critical point*

In this step, the comparison criteria (density, heat capacity and speed of sound) are calculated in the vicinity of the critical point (T=300-310 K, P=7.38 MPa) for all studied EoS. The calculated results are then compared with the experimental data. Absolute relative deviations on density, heat capacity and speed of sound between values predicted by the studied EoS and experimental data are shown in Table 3:

	$\Delta\rho$ (%)	ΔC_p (%)	Δw (%)
SW	13.80	0.51	7.25
PR	10.75	2.21	35.21
SRK	15.04	1.55	41.11
LKP	11.14	1.94	16.41
PR-BM	10.76	2.13	35.21
BWRS	9.42	2.02	18.50

Δ is defined as the mean average of $(property\ value_{experimental} - property\ value_{EoS\ calculated})/property\ value_{experimental}$

Table 3: Relative deviation of experimental data in the critical region from values calculated from different equations of states

Figure 1, Figure 2 and Figure 3 give more details about the studied properties (density, heat capacity and speed of sound, respectively). The experimental data are plotted as function of temperature or pressure in the vicinity of the CO_2 critical point.

a) CO_2 density

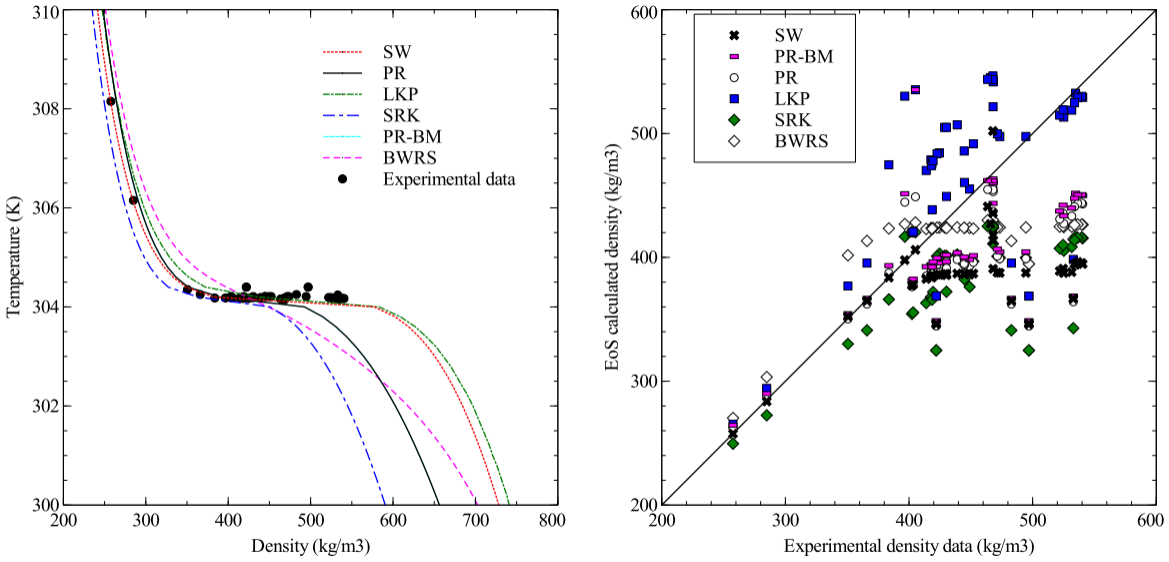

(a) (b)

Figure 1: Representation of isobaric density data in the CO_2 critical region at critical pressure P=7.38 MPa and temperature 300-310 K. (a) The plotted curves correspond to density values calculated from EoS and the black dots correspond to the experimental data, (b) The parity curve of density where EoS calculated value is plotted as a function of experimental data

In terms of density, it is noted that not only the relative deviation but also the shape of the calculated curve is essential to investigate the different EoS. In fact, the BWRS EoS shows a relative small deviation on density (9.5 %) but it does not represent a correct trend of curve (Figure 1 (a)). Moreover, PR, PR-BM, SRK EoS represent important deviations of density in the liquid phase. Only LKP and SW equations have both acceptable deviations and satisfying curve trend comparing to experimental data.

Furthermore, while looking into Figure 1 (b), SW EoS has more points on the parity line (the continuous straight line which represents y=x between experimental data and EoS calculated values).

b) CO_2 heat capacity

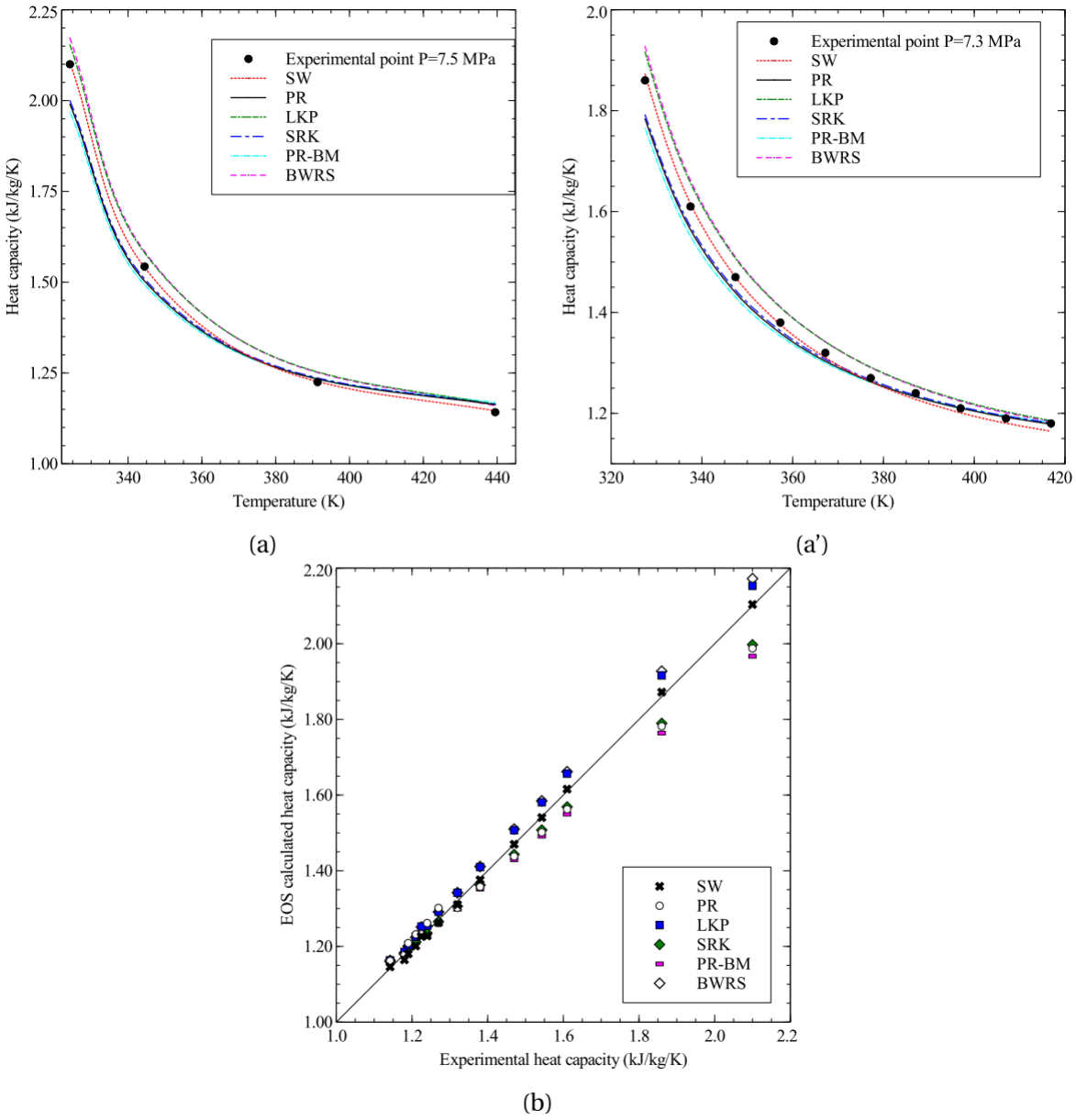

Figure 2: Representation of isobaric heat capacity of the CO_2 in the critical region at: P=7.3 and 7.5 MPa with a temperature around 300-310 K. (a) and (a') The plotted curves correspond to heat capacity values calculated from EoS and the black dots correspond to the experimental data at P=7.5 MPa (a) and P=7.3 MPa (a'). (b) The parity curve of heat capacity where EoS calculated value is plotted as a function of experimental data.

Similar study is carried out for heat capacity. The curve associated with the SW EoS in Figure 2 fits well the experimental data points. Moreover, the collection of the SW EoS points are along the parity line with an average relative deviation as low as 0.51%.

c) CO_2 speed of sound

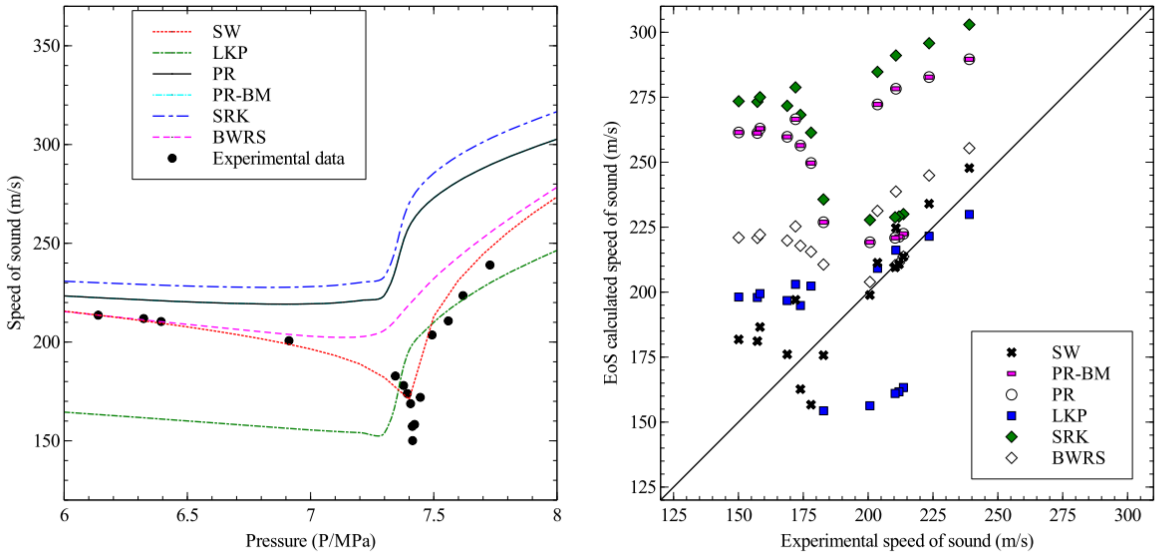

(a) (b)

Figure 3: Representation of isotherm speed of sound in the CO_2 critical region at critical temperature 304 K with a pressure around 6-8 MPa. (a) The plotted curves correspond to values of speed of sound calculated from EoS and the black dots correspond to the experimental data at T_c. (b) The parity curve of speed of sound where EoS calculated value is plotted as a function of experimental data.

The PR, PR-BM, SRK, LKP, BWRS calculated speed of sound profiles are quite different from the experimental data (Figure 3 (a)). In fact, a near-critical fluid is extremely sensitive to pressure and temperature variations. Since the speed of sound depends on derivative of density, it suffers from the large scale fluctuation of density in the vicinity of the critical point. Except for the SW EoS, none of the candidate EoS has considered this phenomena. Thus, only SW equation is the promising candidate for the next step.

3) *Step 3: model/experimental data comparison for the entire region of interest for the SW EoS*

Similarly to previous analysis, this step consists of validating the selected EoS (i.e. the SW EoS) in the entire area of interest (T=300-900 K, P=7-20 MPa) by comparing again the "criteria property" calculations with experimental data. Figure 4, Figure 5 and Figure 6 give more details about the studied criteria. Also, the experimental data are plotted as function of temperature or pressure for the entire area of interest.

a) CO_2 density

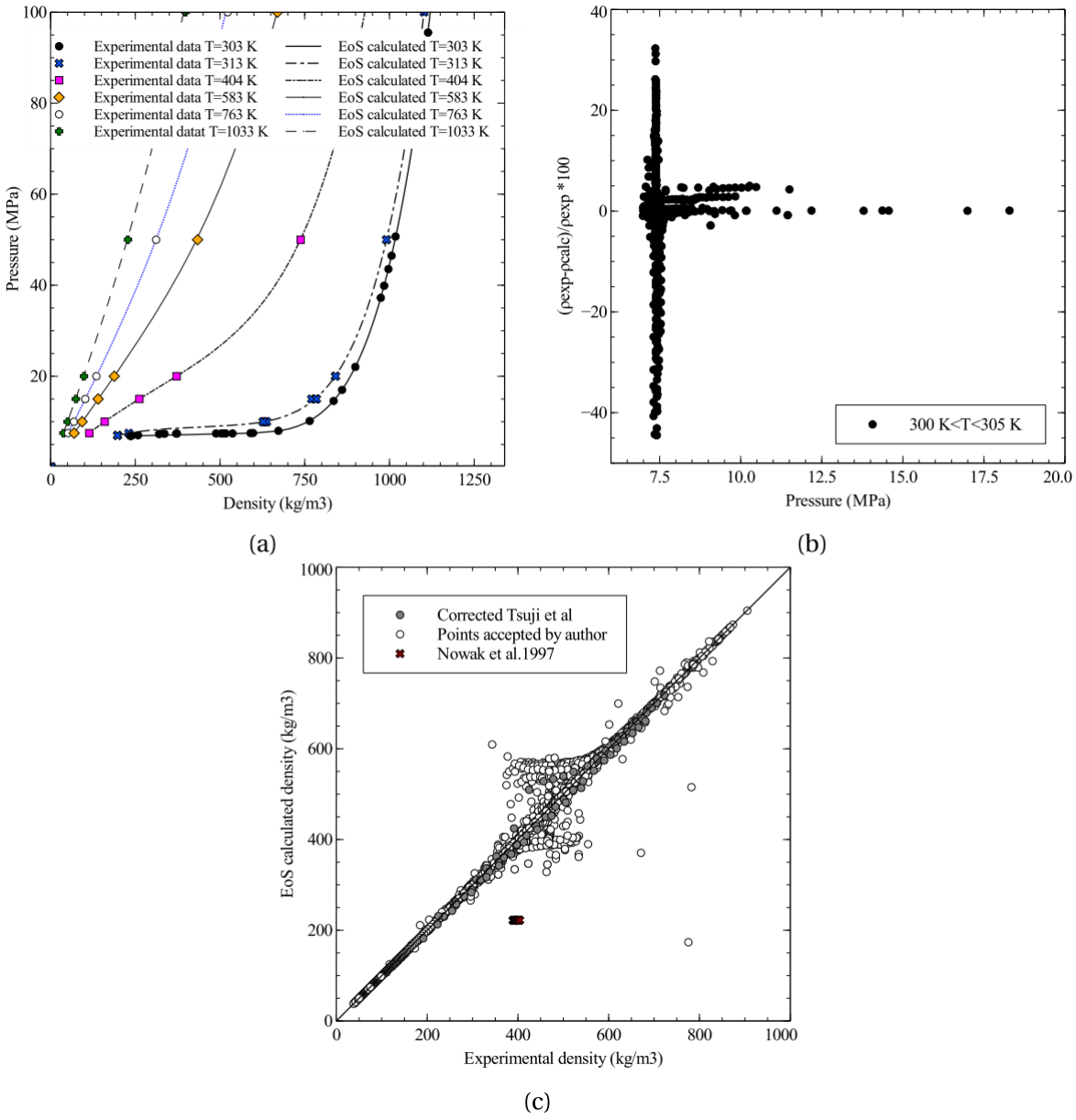

Figure 4: Representation of isotherm density data in the studied range 300 K< T <900 K, 7 MPa< P <20 MPa (a) The plotted curves correspond to density values calculated from the SW equation and the dots correspond to the experimental data at different temperature. (b) Relative deviation between values calculated from the SW equation and experimental data when 300K< T <305 K. (c) parity curve of density where all accessed experimental data are plotted.

Figure 4 shows a good correlation between calculated density from the SW EoS and experimental data, especially at high temperature and pressure. The only area that provides important deviation (> 15 %) is located in the critical region of CO_2, for temperatures in the range 300-305 K and pressures around 7.4 MPa.

b) CO_2 heat capacity

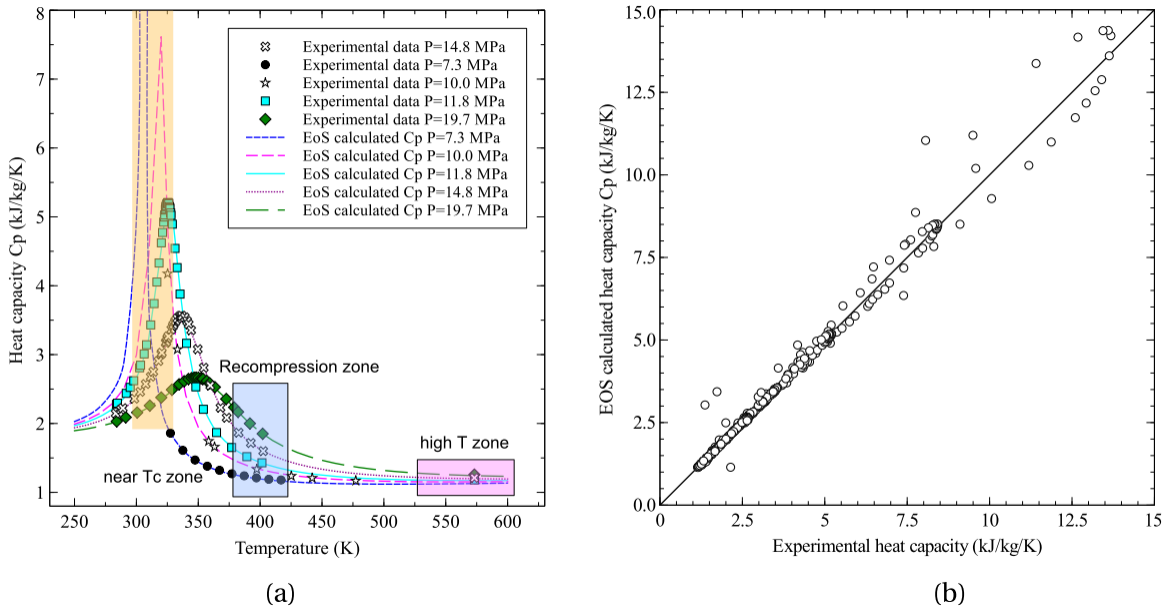

Figure 5: Representation of isobaric heat capacity in the studied range 300 K< T <900 K, 7 MPa< P <20 MPa (a) The plotted curves correspond to heat capacity values calculated from the SW equation and the dots correspond to the experimental data at different pressures. (b) The parity curve of density where all accessed experimental data are plotted.

Figure 5 (a) qualitatively shows that the predicted curves reproduce experimental data with a good accuracy. Note in Figure 5 (b) that the predicted heat capacity points are distributed on the parity line and on both side of the parity line. The observation on relative deviation shows that the most important deviations are located in the vicinity of isobaric curves maxima. In this region, the mean relative deviation is about 30 % while the mean relative deviation considering the entire data set is 1.7 %.

c) CO_2 speed of sound

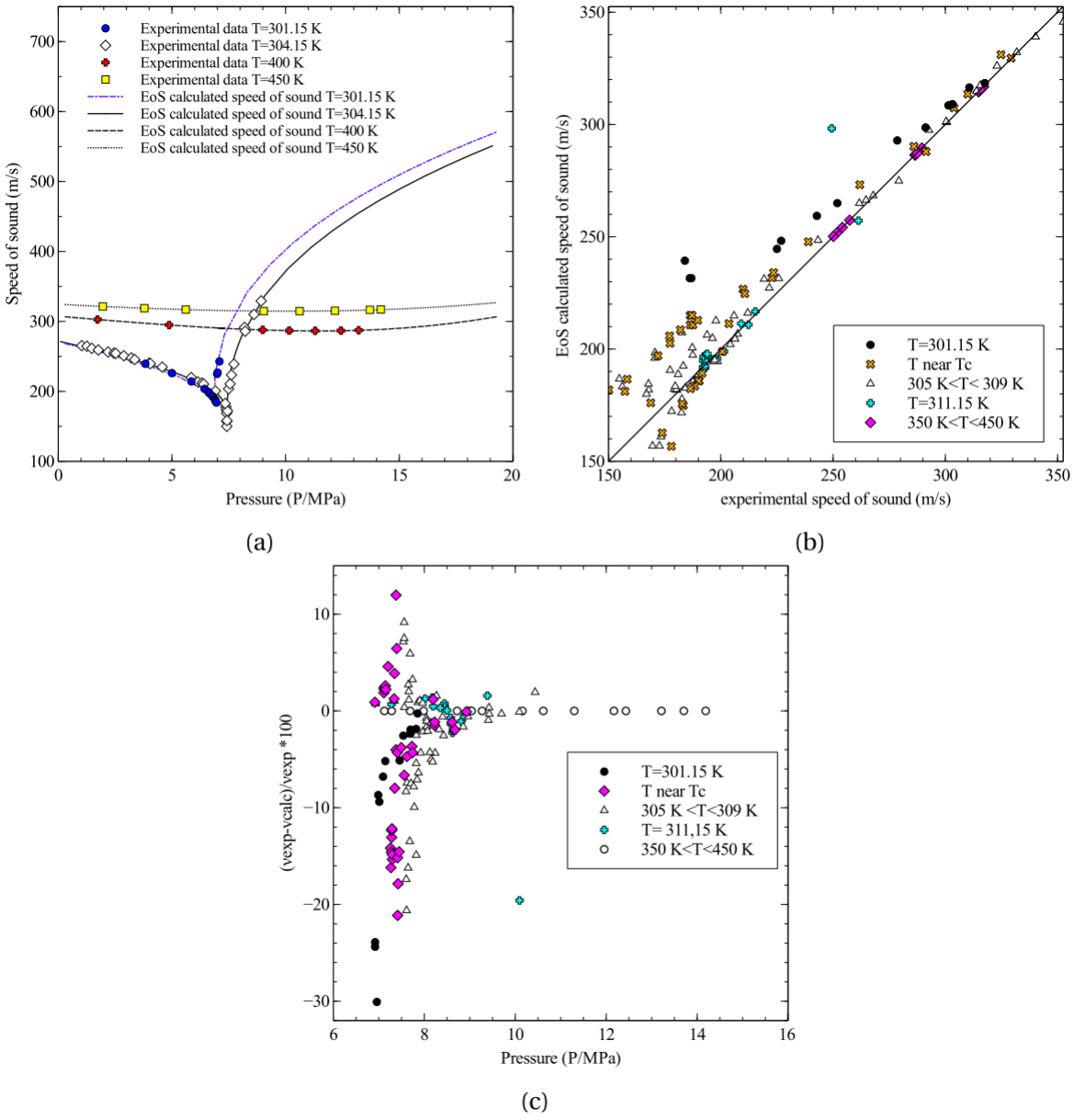

Figure 6: Representation of isotherm speed of sound data in the studied area 300 K< T <900 K, 7 MPa< P <20 MPa (a) The plotted curves correspond to speed of sound values calculated from the SW equation and the dots correspond to the experimental data at different temperatures. (b) Parity curve of density where all accessed experimental data are plotted. (c) Relative deviation between values calculated from the SW equation and experimental data.

As for density and heat capacity, the SW EoS predicted speeds of sound show high correspondence with experimental data, especially at high pressures and temperatures. The mean relative deviation considering the entire data set is 4.8 % and the biggest deviation can be observed around the CO_2 critical point.

This step makes it possible to conclude that the SW EoS is not only interesting near the CO_2 critical point (see step 2) but also presents good accuracy of prediction on all other area of interest.

4) Step 4: comparison of the SW EoS with unused data sets while correlation

Thanks to the step 2 and 3, it is concluded that the SW EoS is able to reproduce accurate predictions of CO_2 properties on all other area of interest. Note that the SW EoS was published in 1994, This step consists of comparing the SW EoS prediction with the latest measured experimental data and some unused data during the construction of SW EoS.

In spite of resurgent interest in measuring the heat capacity and the speed of sound, the lasted data recorded in Detherm database are respectively dated 1995 and 1998. The density is widely applied in both scientific and industrial application thus the latest density data for CO_2 are dated 2013. Table 4 sums up the four latest (appropriate for this study) sets of data and their global deviations.

property	reference	T (K)	P (MPa)	Points	deviation
density	Zolghadr et al. (2013)	313.15-393.15	0.34-17.20	250	3.13%
heat capacity	Dordain et al. (1995)	327-417	5.1-25.8	110	1.40%
speed of sound	Estrada-Alexanders and Trusler (1998)	220-450	0.51-9.27	61	0.02%
	Herget (1940)	301.15-311.15	0.888-10.1	196	3.67%

**deviation is defined as the average of* $(property\ value_{experimental} - property\ value_{SW\ EoS\ calculated})/property\ value_{experimental}$

Table 4: List of experimental data used in step 4

Figure 7 shows the correlation (parity lines) between the latest sets of experimental data shown on Table 4 and the SW EoS calculated values.

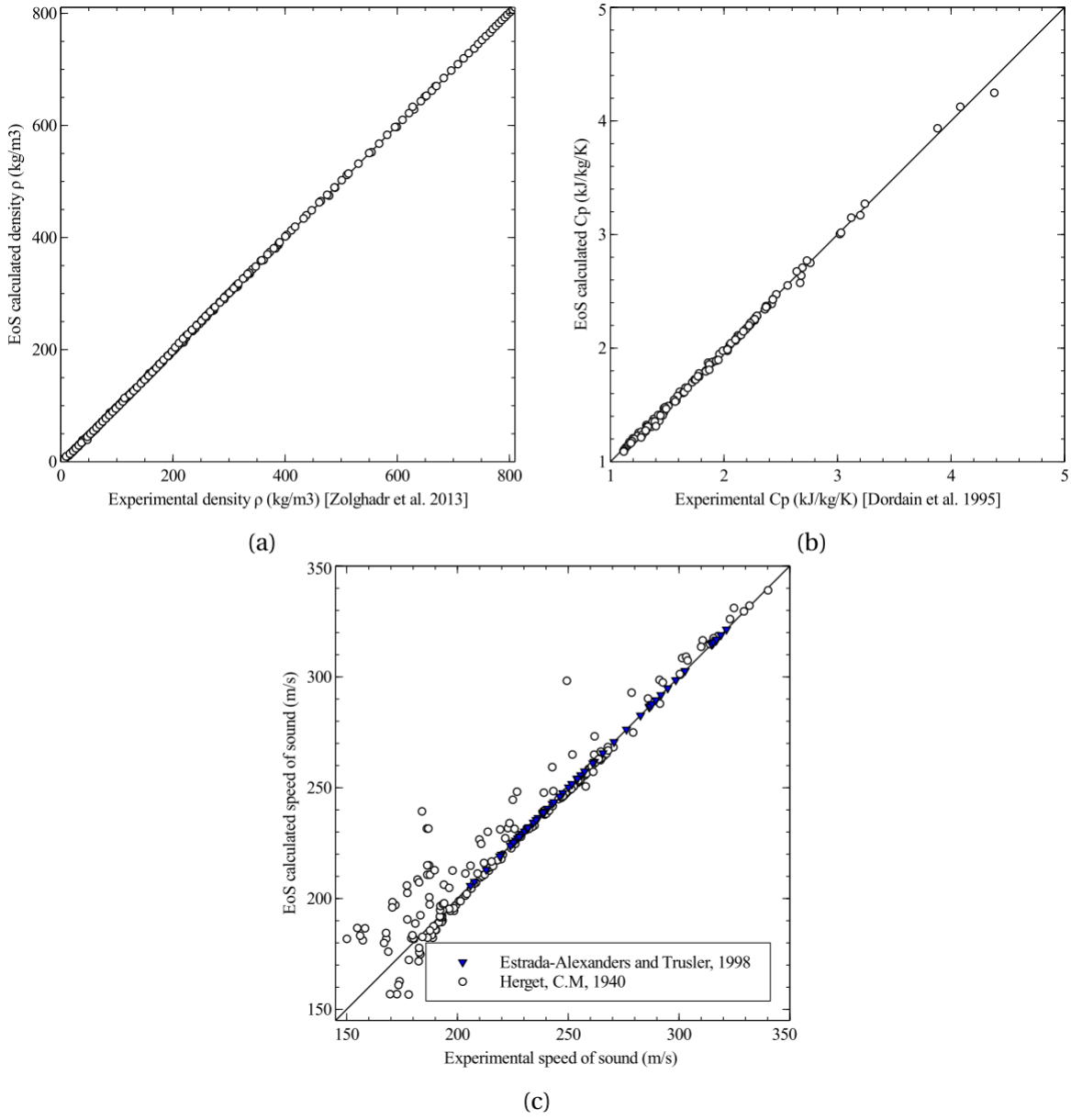

Figure 7: Parity plot of each property (a) density, Zolghadr et al. [2013] (b) heat capacity, Dordain et al. [1995] (c) speed of sound plotted using latest experimental data, Estrada-Alexanders and Trusler [1998], Herget [1940]

Even though the critical point of CO_2 is not always included in the experimental data in Table 4, the good result on parity line implies SW equation generates good prediction on terms of density, heat capacity and speed of sound.

Furthermore, since the measurement uncertainty is rarely provide, it is difficult to have such a discussion on the applied data in this paper. In the paper of Span and Wagner (1994), a thorough comparison was brought out and they have estimated the uncertainty of their equation in different region of temperature and pressure. For more details the reader is recommended to refer to their paper.

CONCLUSION

The choice of the thermodynamic model that can be used to predict the S-CO_2 Brayton cycle performances in the area of interest (T=300-900 K, P=7-20 MPa) has been reviewed and discussed. Our investigations show that the Span-Wagner (SW) EoS is the most accurate in the subcritical, supercritical and critical regions among the six studied EoS. Furthermore, the relative deviation compared to latest experimental database is less than 5 % in global region and less than 15 % in the critical region. In this context, the SW EoS turns to be the best model (among the six studied EoS) to predict the CO_2 behavior in wide area of temperature and pressure, including the supercritical region and the vicinity of its critical point.

Thus, the SW EoS will be used to evaluate the performances of a S-CO_2 Brayton cycle.

Annexes

1) Heat capacity in SRK, PR, PR-BM, BWRS and LKP

The heat capacity of real gas is defined as following:

$$C_p^*(T^*,\, v^*) = C_p^\bullet(T^*,\, v^*) + C_p^{var}(T^*,\, v^*)$$

With
$$\begin{cases} s^{var}(T,\, v) = -\left[\frac{\partial a^{var}(T,\, v)}{\partial T}\right]_v \\ P^{var}(T, v) = -\left[\frac{\partial a^{var}(T,\, v)}{\partial v}\right]_T \\ u^{var}(T,\, v) = a^{var}(T,\, v) + T \cdot s^{var}(T,\, v) \\ C_v^{var}(T,\, v) = \left[\frac{\partial u^{var}(T,\, v)}{\partial T}\right]_v \\ C_p^{var}(T,\, v) = C_v^{var} - T\frac{\left[\left(\frac{\partial P^{var}(T,\, v)}{\partial T}\right)\right]^2}{(\frac{\partial P^{var}(T,\, v)}{\partial v})_T} \end{cases}$$

Where the heat capacity of perfect gas is correlated as (DIPPR, 2016):

$$C_p^\bullet = A + B(\frac{\frac{C}{T}}{sinh(\frac{C}{T})})^2 + D(\frac{\frac{E}{T}}{cosh(\frac{E}{T})})^2$$

With
$$\begin{cases} A = 29370 \\ B = 34540 \\ C = 1428 \\ D = 26400 \\ E = 588 \end{cases}$$

2) Calculation of Cp in SW EoS is defined as following, (Span and Wagner, 1996):

$$\frac{c_p}{R} = \underbrace{-\tau^2(\varphi^\circ{}_{\tau\tau} + \varphi^r_{\tau\tau})}_{\frac{c_v}{R}} + \underbrace{\overbrace{\frac{(1 + \delta\varphi^r_\delta - \delta\tau\varphi^r_{\delta\tau})^2}{1 + 2\delta\varphi^r_\delta + \delta^2\varphi^r_{\delta\delta}}}^{\approx(\frac{\partial p}{\partial T})^2_\rho}}_{\approx(\frac{\partial p}{\partial \rho})_T}$$

3) Calculation of speed of sound for in the SRK, PR, PR-BM, BWRS and LKP EoS:

$$w = \sqrt{(\frac{\partial P}{\partial \rho})_s}$$

4) Calculation of speed of sound in SW EoS:

$$\frac{w^2}{RT} = \underbrace{1 + 2\delta\varphi^r_\delta + \delta^2\varphi^r_{\delta\delta}}_{\approx(\frac{\partial p}{\partial \rho})_T} - \frac{\overbrace{(1 + \delta\varphi^r_\delta - \delta\tau\varphi^r_{\delta\tau})^2}^{\approx(\frac{\partial p}{\partial T})^2_\rho}}{\underbrace{\tau^2(\varphi^\circ{}_{\tau\tau} + \varphi^r{}_{\tau\tau})}_{-\frac{c_v}{R}}}$$

NOTATIONS

Latin symbols

a	Attractive parameter of a cubic EoS (J m^3mol^{-2}) or Helmholtz energy (J mol^{-1})
a_i	Coefficient in SW EoS (-)
$a', b', c', d', e', f', g', h'$	Coefficients of BWRS EoS (-)
A_i	Coefficient in SW EoS (-)
A_j	Universal coefficients in BWRS EoS (-)
b	Covolume (m^3mol^{-1})
b_i	Coefficient in SW EoS (-)
B_i	Coefficient in SW EoS (-)
B_j	Universal coefficients in BWRS EoS (-)
b_{1-4}, c_{1-4}	Universal coefficients in LKP EoS (-)
c	Parameter of Boston-Mathias alpha function (-)
c_i	Coefficient in SW EoS (-)
c_v	Specific heat at constant volume (kJ $kg^{-1}K^{-1}$)
c_p	Specific heat at constant pressure (kJ $kg^{-1}K^{-1}$)
d	Parameter of Boston-Mathias alpha function (-)
d_1, d_2	Universal coefficients in LKP EoS (-)
d_i	Coefficient in SW EoS (-)
L, M, N	Parameters of the Twu alpha function (-)
m	Parameter of the Soave alpha function (-)
M	Molar mass (kg/mol)
n_i	Coefficient in SW EoS (-)
P	Pressure (Pa)
R	Gas constant (J $mol^{-1}K^{-1}$)
t_i	Coefficient in SW EoS (-)
T	Absolute temperature (K)
v	Molar volume (m^3mol^{-1})
w	Speed of sound (ms^{-1})
Z	Compressibility factor (-)

Greek letters

α	Alpha function of cubic EoS (-)
α', γ'	Coefficient in BWRS EoS (-)
α_i	Coefficient in SW EoS (-)
β_i	Coefficient in SW EoS (-)
β	Universal coefficient in LKP EoS (-)
ϵ_i	Coefficient in SW EoS (-)
γ	Universal coefficient in LKP EoS (-)
γ_i	Coefficient in SW EoS (-)
ρ	Masse volumique ($kg.m^{-3}$)
τ	Inverse reduced temperature in SW EoS(-)
δ	Reduced density in SW EoS (-) or the mean deviation between calculated and experimental value
Δ	Distance function defined in SW EoS (-)
ω	Pure-component acentric factor (-)
φ	Dimensionless Helmholtz function (-)

Subscript

c	Critical property
r	Reduced property
R	Reference fluid
T	Isotherm property
S	Isentropic property
ρ	Density constant property

Exponents

0	Simple fluid
o	Ideal-gas part
$*$	Real fluid
R	Reference fluid
dep	Departure function

Acronym

BM	Boston-Mathias alpha function
BWR	Benedict-Webb-Rubin
BWRS	Benedict-Webb-Rubin modified by Starling-Nishiumi
EoS	Equation of state
LKP	Lee-Kesler-Plöcker
vdW	Van der Waals
P-v-T	Pressure-Volume-Temperature
PR	Peng-Robinson
RK	Redlich-Kwong
SAFT	Statiscal associating fluid theory
S-CO_2	Supercritical CO_2
SRK	Soave modified Redlich-Kwong
SW	Span-Wagner

REFERENCES

M. Benedict, G.B. Webb, and L.C. Rubin. An Empirical Equation for Thermodynamic Properties of Light Hydrocarbons and Their Mixtures II. Mixtures of Methane, Ethane, Propane, and n-Butane. The Journal of Chemical Physics, 10(12):747–758, 1942.

F.J. Blas and L.F. Vega. Thermodynamic behaviour of homonuclear and heteronuclear Lennard-Jones chains with association sites from simulation and theory. Molecular Physics, 92(1):135–150, 1997.

Detherm database, 2016. URL http://www.dechema.de/Detherm.html.

DIPPR, 2016. URL http://www.aiche.org/dippr/events-products/801-database.

L. Dordain, J.Y. Coxam, J.R. Quint, J.P.E. Grolier, E.W. Lemmon, and S.G. Penoncello. Isobaric heat capacities of carbon dioxide and argon between 323 and 423 K and at pressures up to 25 MPa. Journal of Supercritical Fluids, 8(3):228–235, 1995.

A.F. Estrada-Alexanders and J.P.M. Trusler. Speed of sound in carbon dioxide at temperatures between (220 and 450) K and pressures up to 14 MPa. Journal of Chemical Thermodynamics, 30(12):1589–1601, 1998.

A. Gil-Villegas, A. Galindo, P.J. Whitehead, S.J. Mills, G. Jackson, and A.N. Burgess. Statistical associating fluid theory for chain molecules with attractive potentials of variable range. The Journal of Chemical Physics, 106(10):4168–4186, 1997.

J. Gross, and G. Sadowski. Perturbed-chain saft: An equation of state based on a perturbation theory for chain molecules. Industrial & Engineering Chemistry Research, 40(4):1244–1260, 2001.

C.M. Herget. Ultrasonic velocity in carbon dioxide and ethylene in the critical region. Journal of Chemical Physics, 8(7):537–542, 1940.

Y. Kim. Equation of state for carbon dioxide. Journal of Mechanical Science and Technology, 21(5):799–804, 2007.

M. Mazzoccoli, B. Bosio, E. Arato, and S. Brandani. Comparison of equations-of-state with P-ρ-T experimental data of binary mixtures rich in CO_2 under the conditions of pipeline transport. Journal of Supercritical Fluids, 95:474–490, 2014.

P. Nowak, Th. Tielkes, R. Kleinrahm, and W. Wagner. Supplementary measurements of the (p,rho,t) relation of carbon dioxide in the homogeneous region at T=313 K and on the coexistence curve at T=304 K. The Journal of Chemical Thermodynamics, 29(8):885 – 889, 1997.

H. Nushiumi and S. Saito. An improved generalized bwr equation of state applicable to low reduced temperatures. Journal of Chemical Engineering of Japan, 8(5):356–360, 1975.

D. Peng and D. Robinson. A new two-constant equation of state. Industrial & Engineering Chemistry Fundamentals, 15(1):59–64, 1976.

K.S. Pitzer and R.F. Curl. The volumetric and thermodynamic properties of fluids. iii. Empirical equation for the second virial coefficient 1. Journal of the American Chemical Society, 79(10):2369–2370, 1957.

G. Soave. Equilibrium constants from a modified Redlich-Kwong equation of state. Chemical Engineering Science, 27(6):1197–1203, 1972.

R. Span and W. Wagner. A new equation of state for carbon dioxide covering the fluid region from the triple-point temperature to 1100 K at pressures up to 800 MPa. Journal of Physical and Chemical Reference Data, 25(6):1509–1558, 1996.

T. Tsuji, S. Honda, T. Hiaki, and M. Hongo. Measurement of the p -v-t relationship for carbon dioxide+n-butane and carbon dioxide+i-butane in the vicinity of the critical point. The Journal of Supercritical Fluids, 13(1):15–21, 1998.